

Influence of Composition, pH, Annealing Temperature, Wave Form, and Frequency on Structure and Magnetic Properties of Binary $\text{Co}_{1-x}\text{Al}_x$ and Ternary $(\text{Co}_{0.97}\text{Al}_{0.03})_{1-x}\text{Fe}_x$ Nanowire Alloys

Mojgan Najafi¹

Received: 29 February 2016 / Accepted: 21 May 2016 / Published online: 4 June 2016
© Springer Science+Business Media New York 2016

Abstract $\text{Co}_{1-x}\text{Al}_x$ and $(\text{Co}_{0.97}\text{Al}_{0.03})_{1-x}\text{Fe}_x$ nanowire alloys and elemental Co nanowire were prepared in anodic aluminum oxide templates by the electrochemical deposition method. The influence of composition, pH, annealing temperature, wave form, and frequency on structure and magnetic properties of Co/Al/Fe nanowires was studied. The changes in the saturation magnetization, coercivity, remanent squareness, and crystal structure of nanowires with changing of the above parameters were also investigated. The roomtemperature magnetic hysteresis loops show that the coercivity and squareness of the nanowire arrays in parallel to the wire axis change with the changing of the abovementioned parameters, which can be mainly attributed to the strengthening of anisotropy. X-ray diffraction observations demonstrated that the isolated nanowires have a crystalline structure and that their phases change with the annealing temperature. Magnetic measurements, on the other hand, showed that the coercivity reached a maximum value at $x = 0.03$ in the $\text{Co}_{1-x}\text{Al}_x$ nanowires. Also, the coercivity of the $\text{Co}_{1-x}\text{Al}_x$ nanowires was increased with increasing annealing temperature for all the compositions.

Keywords Nanowire arrays · Magnetic properties · Magnetic anisotropy · Electrodeposition · Anodic aluminum oxide membrane

1 Introduction

Recently, the synthesis of one-dimensional nanostructures like nanowires, nanotubes, and nanorods has attracted more and more attentions because of their contribution to the understanding of basic concepts and potential applications in optical [1], electrical [2], and magnetic [3, 4] devices. Among the different approaches in the fabrication of nanowires, the highly ordered porous alumina templates developed by a two-step anodization [5–7] have received considerable attention due to its several unique structure properties, such as controllable pore diameter, ideally cylindrical shape of pores, and extremely narrow size distribution for pore diameters.

The earlier investigations indicate that the magnetic nanowire arrays filled in anodic aluminum oxide (AAO) membrane pores make them more suitable for an ideal candidate of perpendicular magnetic recording media [8, 9] because they can achieve a recording density of more than 15.50 Gbit/cm^2 [10].

Electrodepositing the magnetic metal wires with nanoscale into the porous AAO templates has been utilized previously by many groups to prepare the one-dimensional nanostructure alloys [11–17]. Cobalt, a kind of typical ferromagnetic element, has an intensive application in magnetic recording domain, and so far, its arrays have widely been synthesized by various techniques. Over-high and immoderate coercivity of cobalt had made it unsuitable for an ideal candidate of perpendicular recording media. So, it is significant and a challenge for us to reduce the coercivity of the cobalt array so that it can be used as proper magnetic recording media. Recently, ferromagnetic–nonmagnetic alloys have attracted much interest [18–26]. To add a nonmagnetic substance in a magnetic array has been proved to

✉ Mojgan Najafi
mojgannajafi1@gmail.com

¹ Department of Materials Engineering, Hamedan University of Technology (HUT), Hamedan, Iran

be a good technique to regulate the magnetic property of the arrays. So far, many replacements of magnetic metals have been applied to add in the magnetic array, such as Cu [27], Ag [28], Fe [29], Ni [30], and Pt [31]. However, the works have been mainly focused on these metals added in the arrays, and hence, no report have been published regarding Co–Al and Co–Al–Fe alloy systems.

In this paper, we reported that cobalt-doped aluminum and iron nanometer arrays have been fabricated by alternating current (AC) electrodeposition, using the alumina film as a template. Our results show that the crystalline microstructures of the Co/Al- and Co/Al/Fe-deposited nanowires become more different with Co and their magnetic properties. The deposition process and the dependence of alloy composition on the concentration ratio of Co, Al, and Fe in the solution have been examined for the fabrication of Co–Al and Co–Al–Fe alloy nanowires. The structure of the nanowires has been investigated using conventional X-ray diffraction (XRD) and scanning electron microscopy (SEM), while the magnetic properties have been measured using an alternating gradient force magnetometer (AGFM).

2 Experimental

Aluminum foils, with purities of 99.99 % and 0.30 mm thickness, were degreased and electropolished in a mixture of perchloric acid (HClO_4) and ethanol $\text{C}_2\text{H}_5\text{OH}$ by applying a constant voltage of 20 V for 9 min and magnetic stirring in order to reduce the surface roughness, before it was placed in an anodization cell.

The two-step anodization process was carried out in constant voltage mode to improve the arrangement of the ordered nanopore arrays. In the first step of the anodization, aluminum foil was anodized in a 0.3 M oxalic acid solution at 17 °C under a constant voltage of 40 V for 15 h, resulting in a textured surface, and then the formed anodic alumina layer was removed in a mixed solution of 0.5 M phosphoric acid and 0.2 M chromic acid at 70 °C for 15 h [32, 33]. Subsequently, the foil was re-anodized for 1 h using the same parameters as in the first step. After anodization, a technique of reducing the anodization voltage to 8 V in a series of small steps was applied to thin the barrier layer in order to increase the deposition rate. The voltage variation was performed in a stepwise manner; e.g., for a 40 to 20 V region, the voltage was kept at an appropriate value for 30 s. Then, it was immediately fallen to its next down-step value (2 V lower). This procedure was repeated for the next region with step changes of 1 V and then 0.5 V.

The electrodeposition was performed by using a standard double-electrode bath. The AAO template was used as one electrode and a piece of Pt as another. The Co–Al and

Co–Al–Fe alloys were electrodeposited in the pores of the alumina templates using the potentiostatic method at a constant potential. The voltage used in the AC electrodeposition was 30.0 V.

The electrolyte used to electrodeposit the Co–Al and Co–Al–Fe nanowires had the following composition, respectively: (a) M of $\text{CoSO}_4 \cdot 7\text{H}_2\text{O}$ and (b) M of $\text{Al}_2(\text{SO}_4)_3 \cdot 18\text{H}_2\text{O}$ and H_3BO_3 and (a) M of $\text{CoSO}_4 \cdot 7\text{H}_2\text{O}$, (b) M of $\text{Al}_2(\text{SO}_4)_3 \cdot 18\text{H}_2\text{O}$, and (c) M of $\text{FeSO}_4 \cdot 7\text{H}_2\text{O}$ and H_3BO_3 . The pH of aqueous bath was adjusted by adding appropriate amounts of dilute HCl or NaOH.

A series of $\text{Al}_2(\text{SO}_4)_3 \cdot 18\text{H}_2\text{O}$ and $\text{FeSO}_4 \cdot 7\text{H}_2\text{O}$ salts were added to fabricate the Co–Al and Co–Al–Fe nanowire arrays with various components. After deposition, some of the samples were annealed at different temperatures (200, 400, 500, and 550 °C) in the Ar inert atmosphere for 20 min and then slowly cooled down to a room temperature. The resulted products were observed by means

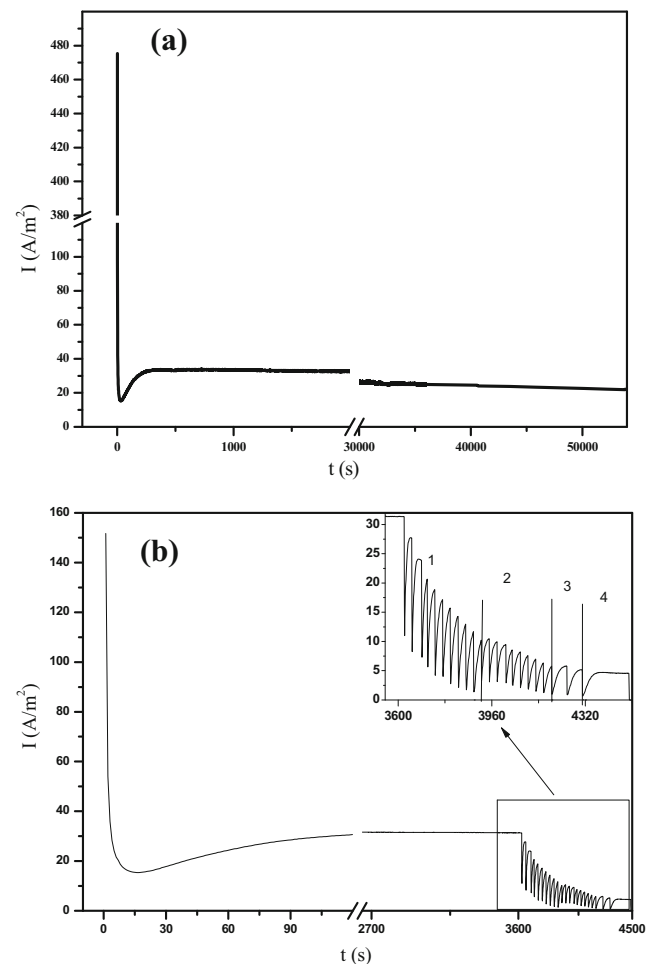


Fig. 1 (a) Chronoamperometric curve during first anodization of Al in 0.3 M oxalic acid at 40 V and at 17 °C; (b) current in the second anodizing and thinning barrier layer process

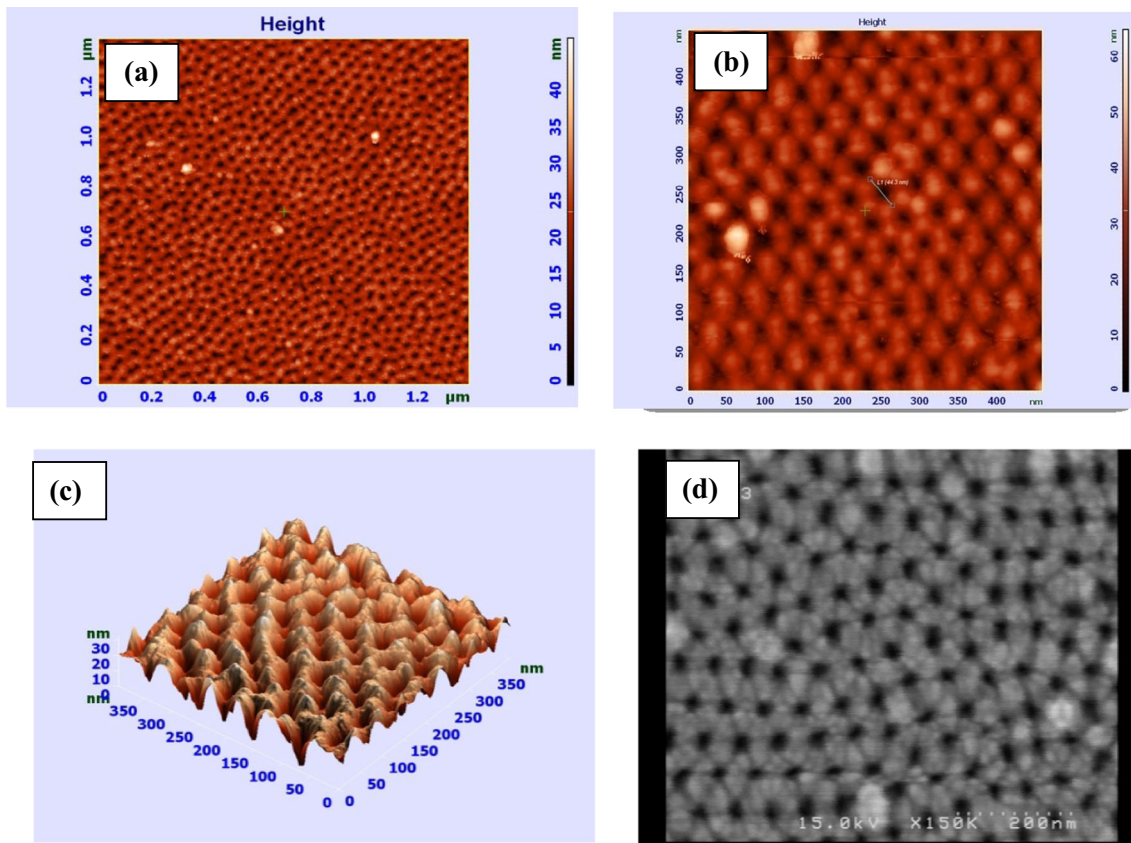


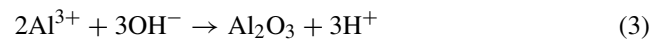
Fig. 2 AFM images of the textured Al surface: **a, b** after the first anodization,; **c** after the second anodization, and **d** SEM image of the Al surface after the second anodization

of SEM (Philips SEM XL30 microscope operating at 30 kV) and atomic force microscopy (AFM; NT-NDT, Russia). The XRD instrument (Ital Structures model APD2000 with the applied Cu $K\alpha$ radiation wavelength ≈ 0.15405 nm) was employed to investigate the microstructure of the as-obtained arrays. The magnetic properties of the as-obtained nanowires were measured by the AGFM at room temperature. The applied magnetic field was 10 kOe. All experiments were carried out at room temperature.

3 Results and Discussion

An anodic aluminum oxide film was grown by two-step anodization in oxalic acid solution at 40 V. The current density–time transient during first and second anodizations

of the AAO template is given in Fig. 1. The anodic reaction is given in (1) to (3)



For which, the overall process is



The cathodic reaction is as follows:

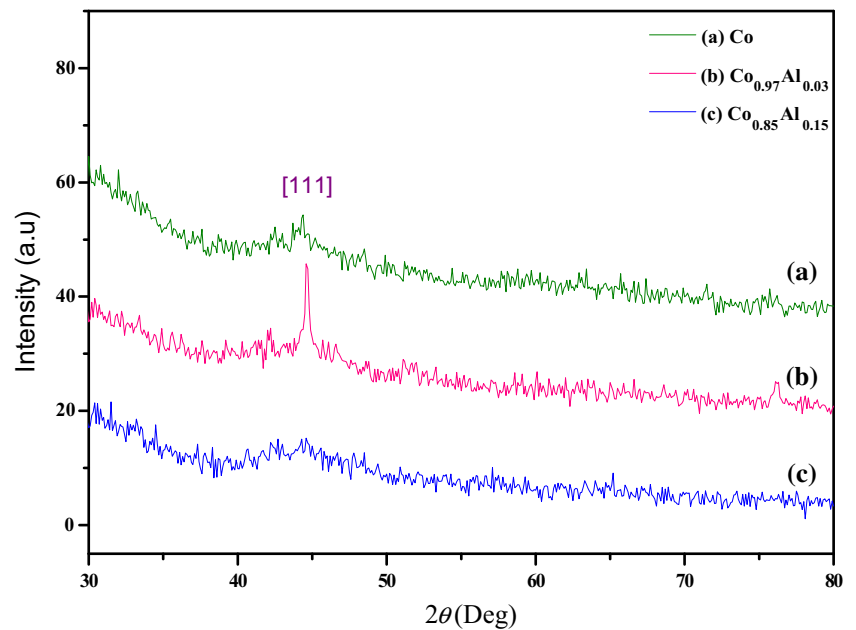


Figure 2 shows the AFM and SEM images of the AAO template prepared by the two-step anodic oxidation. It can

Table 1 The composition of the electrolyte used for electrodeposition of $\text{Co}_{1-x}\text{Al}_x$ nanowires

Sample	Co	$\text{Co}_{0.99}\text{Al}_{0.01}$	$\text{Co}_{0.97}\text{Al}_{0.03}$	$\text{Co}_{0.95}\text{Al}_{0.05}$	$\text{Co}_{0.90}\text{Al}_{0.10}$	$\text{Co}_{0.85}\text{Al}_{0.15}$
Concentration of $\text{CoSO}_4 \cdot 7\text{H}_2\text{O}$ (g/l)	281.1	278.2	272.7	267.0	253.0	238.9
Concentration of $\text{Al}_2(\text{SO}_4)_3 \cdot 18\text{H}_2\text{O}$ (g/l)	0.0	3.3	10.0	16.7	33.3	50.0

Fig. 3 *a–c* XRD patterns of Co, $\text{Co}_{0.97}\text{Al}_{0.03}$, and $\text{Co}_{0.85}\text{Al}_{0.15}$ nanowires without annealing



be seen that the template exhibits a highly ordered array with a circular structure. The average diameter of the pores is 44.3 nm, and the distance between the pores is close to 49.9 nm. The aspect ratio of the holes (depth to diameter) is great (more than 55). At the same time, the parameters above are easily regulated by altering the conditions of anodic oxidation.

Co, $\text{Co}_{1-x}\text{Al}_x$, and $(\text{Co}_{0.97}\text{Al}_{0.03})_{1-x}\text{Fe}_x$ nanowires were fabricated using electrodeposition and homemade AAO. Porous aluminum oxide on aluminum was used as a working electrode. For electrodeposition of Co, the electrolyte solution consisted of 0.3 M $\text{CoSO}_4 \cdot 7\text{H}_2\text{O}$ and 45 g/l⁻¹ oric acid (as a catalyst and buffer). $\text{Co}_{1-x}\text{Al}_x$ nanowires were electrodeposited from five different electrolytes. Table 1 lists the concentration of the ions in these five electrolytes

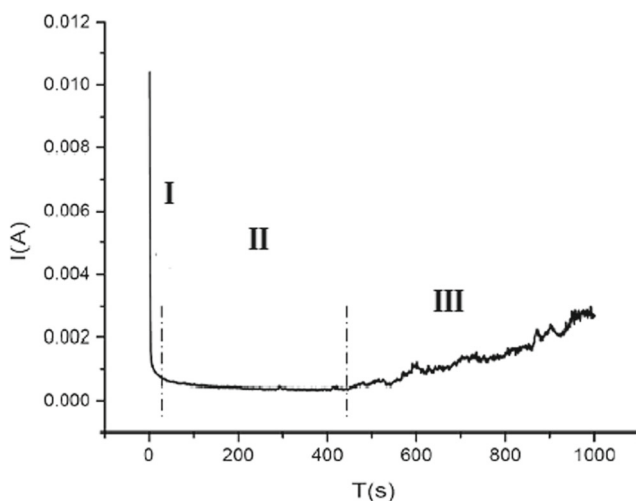


Fig. 4 Typical electrodeposition current versus time has three parts

that were used for electrodeposition. The pH value of the electrolyte solution was maintained at adjusted values. In the first step, the electrodeposition frequency and electrodeposition peak-to-peak voltage were maintained at 200 Hz in sine wave form and 30 V_{pp}, respectively.

The X-ray diffraction patterns of AAO templates filled with Co, $\text{Co}_{0.97}\text{Al}_{0.03}$, and $\text{Co}_{0.85}\text{Al}_{0.15}$ nanowires are shown in Fig. 3. The result shows that there is a diffraction peak corresponding to a face-centered cubic (fcc) structure of Co when the Al content ranges from 0 to 15 %. The XRD pattern shows that the $\text{Co}_{1-x}\text{Al}_x$ nanowires comprise of fcc

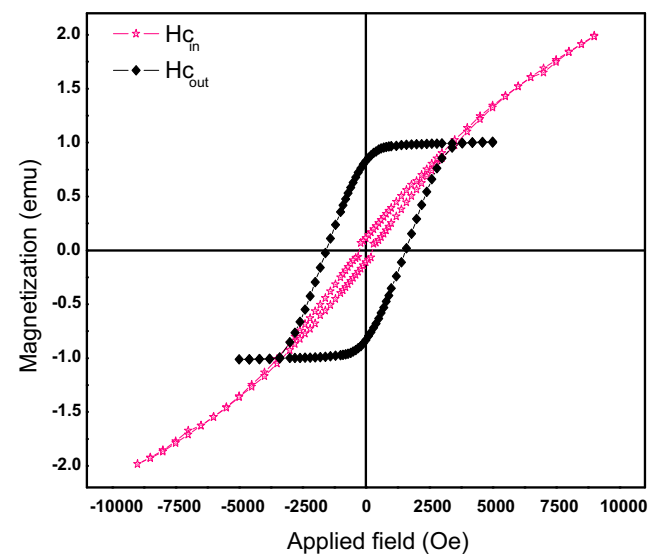
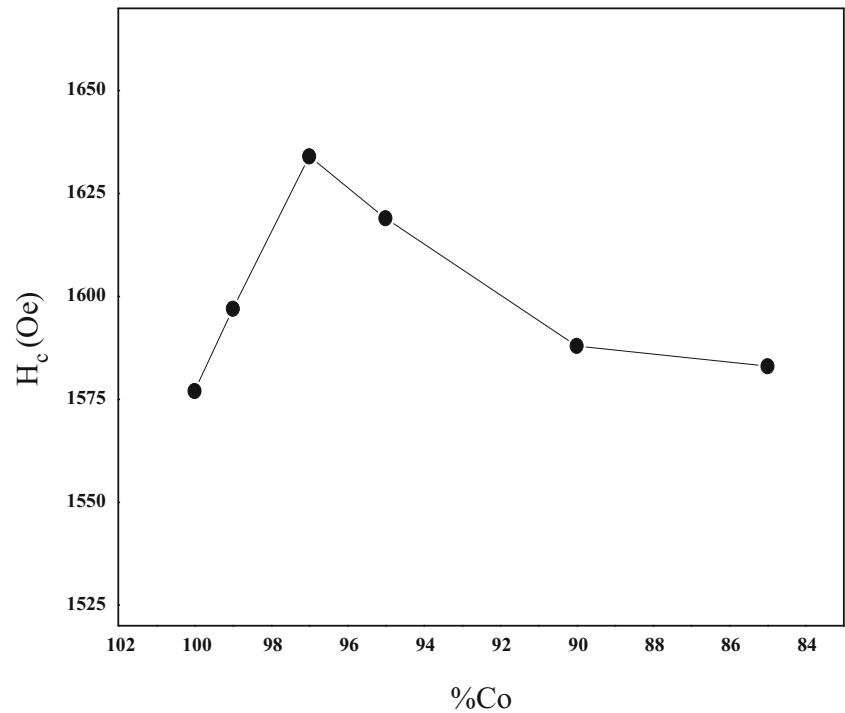


Fig. 5 Hysteresis loops of the $\text{Co}_{0.97}\text{Al}_{0.03}$ nanowire electrodeposited at 200 Hz with sine wave form in the AAO template. *Out* and *in* represent that the applied field is parallel and perpendicular to the long axis of nanowires, respectively

Fig. 6 Coercivity (H_c) of the samples with different Co concentrations in the $\text{Co}_{1-x}\text{Al}_x$ nanowires deposited at 200 Hz and 30 Vpp in sine wave form

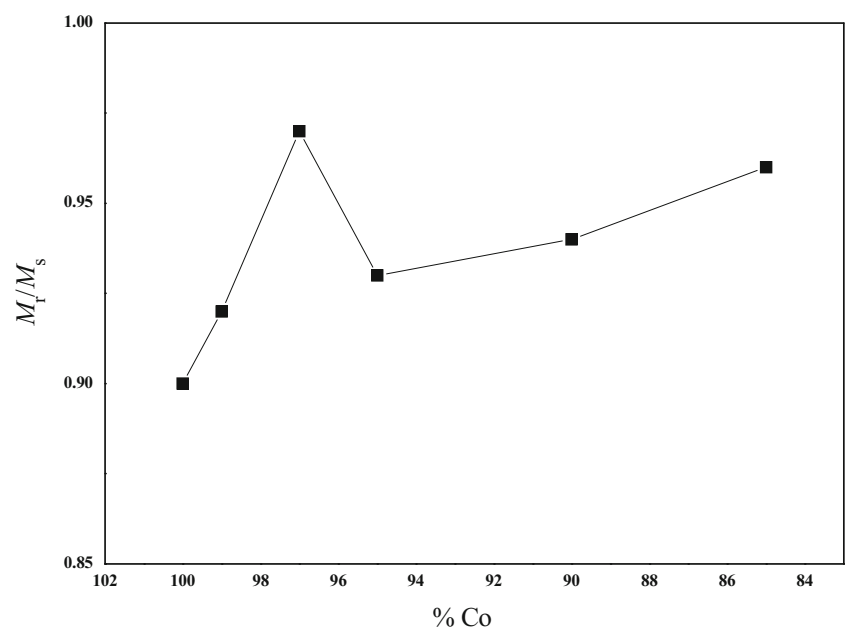


phase with the identifiable most intensive diffraction peak, namely (111).

We found that electrodeposition of metal nanowires changes the color of the template from goldish to black. So, the black color indicates the nucleation and growth of the nanowires. A profile of typical electrodeposition current versus time is shown in Fig. 4. The horizontal part of the current transient indicates the production of nanowires in the pores of the alumina membrane. Current variation also

shows that there is no over-deposition and that the nanowire is in the growth state [34]. This electrodeposition current can be established in three parts: (1) the current starts off high due to the reduction of the cations at the base of the pores. Almost immediately thereafter, the current drops and the small nanopore at the bottom of the main pore is filled rapidly (during several second). It has been suggested that deposition in narrow- and high-aspect-ratio channels may drive the deposition to become diffusion-limited; (2) in the

Fig. 7 Squareness of the as-deposited $\text{Co}_{1-x}\text{Al}_x$ nanowires as a function of Co concentration



second part, the aligned main pores are filled with constant current; and (3) when over-growth begins, the current density increases because of lessened diffusion limitations.

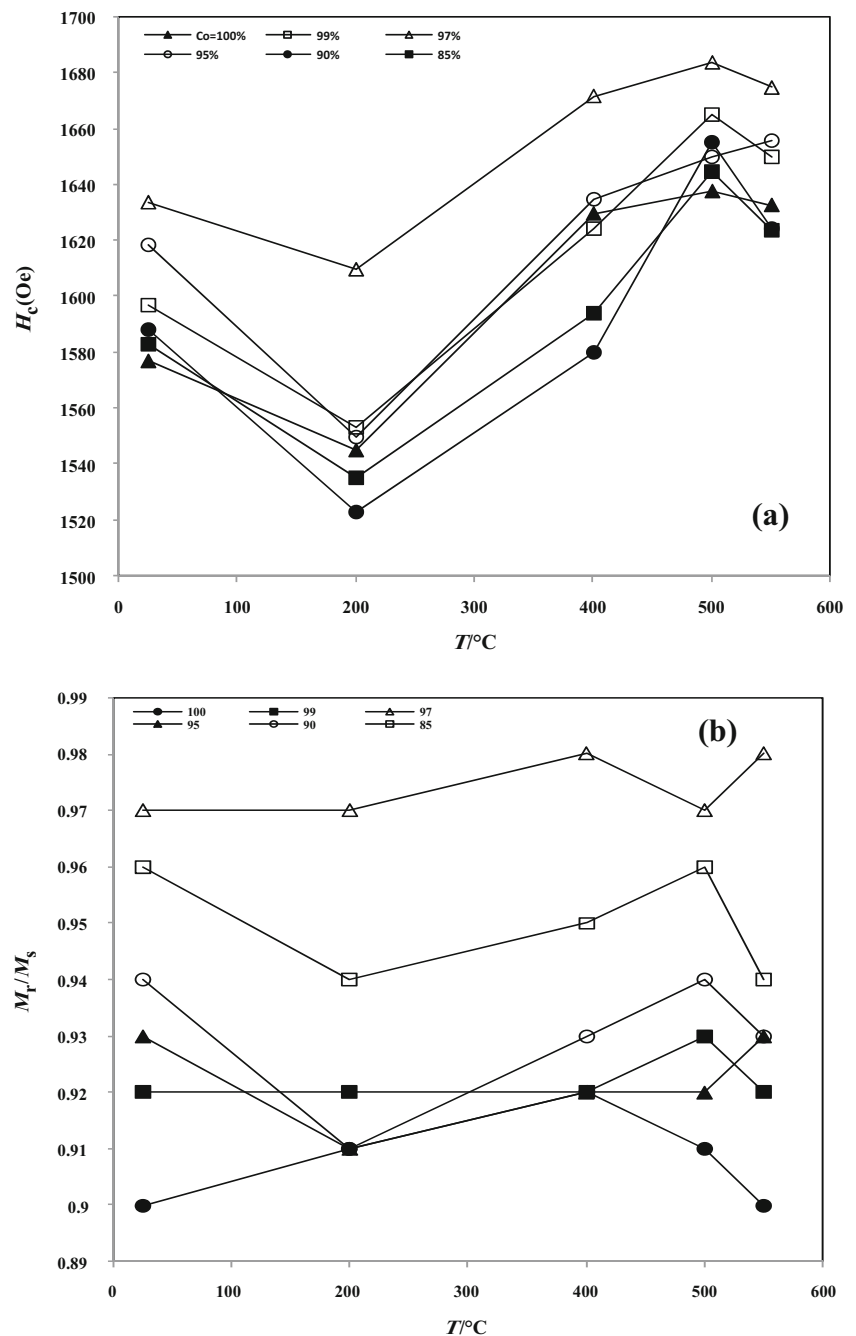
Hysteresis loops were measured at various conditions such as metal composition, annealing temperature, pH, electrodeposition frequency, and wave form for nanowires in the parallel and perpendicular geometries.

Figure 5 shows the typical hysteresis loops of $\text{Co}_{0.97}\text{Al}_{0.03}$ nanowire array at room temperature. The external field was applied parallel (\parallel) and perpendicular (\perp) to the long axes of the nanowires which were not removed

from the membrane. From Fig. 5, due to the marked differences of coercivity values for out-of-plane $H_c(\parallel)$ and in-plane $H_c(\perp)$, we can conclude that $\text{Co}_{1-x}\text{Al}_x$ nanowire arrays have strong magnetic anisotropy with preferential magnetic orientation (easy axis of magnetization) being parallel to the longitudinal wire axis.

It is well known that the magnetic anisotropy originates from several factors: magnetocrystalline, shape, and stress anisotropies. It has also been reported [35, 36] that because of the strong shape anisotropy, nanowire arrays exhibit uniaxial magnetic anisotropy with respect to the

Fig. 8 **a** Coercivity and **b** squareness of $\text{Co}_{1-x}\text{Al}_x$ nanowires as a function of annealing temperature. The samples were annealed for 20 min at different temperatures. All measurements were performed at room temperature with the field applied along the nanowires



easy magnetization direction along the nanowire axes. So, a very different magnetization of nanowires along in-plane in comparison with that along out-of-plane in the present work probably is due to the predominant shape anisotropy contribution.

Also, Fig. 6 illustrates the coercivity of the as-deposited $\text{Co}_{1-x}\text{Al}_x$ alloy nanowires measured at room temperature. Compared with the pure Co nanowires that have an out-of-plane coercivity of 1600 Oe at a similar condition, the coercivity of these alloy nanowires changed with a small amount of Al component. The magnetic properties of the samples with different concentrations of Al^{3+} ions in the electrolyte were measured. It can be seen that the out-of-plane coercivity of nanowires dramatically changes with increasing of the aluminum concentration in the solution. Coercivity considerably increases with the addition of a small amount of aluminum as small as 3 % to the solution. It then decreases by more increasing of the Al concentration up to about 15 %. The anisotropy is associated with the distribution of easy axis, which has a tendency to lie along the wire axis.

On the other hand, different behaviors are observed for a variation of squareness with increasing the Al concentration (Fig. 7). As shown, the out-of-plane squareness is increased from 0.90 for Co nanowires to 0.97 for nanowires with 3 % of Al concentration. However, the value of squareness is decreased for nanowire samples made from solution with higher concentration to 0.93 for 5 % and then increased with more addition of Al concentration, i.e., 0.94 for 10 % and 0.96 for 15 %.

Figure 8a, b shows the dependence of coercive field and squareness as a function of the annealing temperature for $\text{Co}_{1-x}\text{Al}_x$ nanowires annealed for 40 min in Ar atmosphere, when the external magnetic field is applied along the wires. We suggest that the change of magnetic properties after annealing is related to microstructural changes during the annealing process. For all samples, the coercive field increases rapidly and reaches a maximum for the samples annealed at 500 °C. As seen in Fig. 8a, the coercive field drops for higher annealing temperatures (> 500 °C). The enhancement in coercive field and squareness could be due to a better alignment between the easy axis and the nanowire axis or a better distribution of secondary phases. On the other hand, the degradation in magnetic properties noticed for higher annealing temperature (> 500 °C) may be associated with the appearance of free aluminum and disappearance of the Co–Al phase.

The magnetic properties of $\text{Co}_{0.95}\text{Al}_{0.05}$ nanowires electrodeposited at different frequencies of 50–500 Hz as well as different wave forms were studied. All samples were electrodeposited for 2 min. Figure 9 shows the out-of-plane $H_c(\parallel)$ coercivity of the samples against frequency for three different wave forms, i.e., sine, triangle, and square

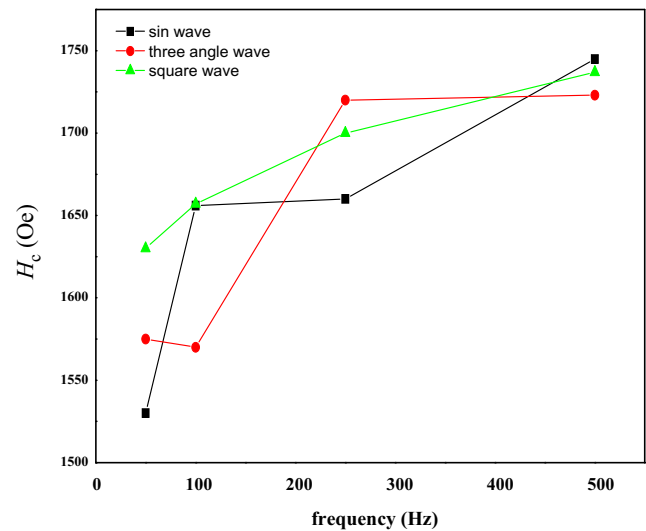


Fig. 9 Coercivity of $\text{Co}_{0.95}\text{Al}_{0.05}$ nanowires as a function of frequency for three different wave forms

wave forms. As can be seen, the coercivity of the samples increased with increasing the frequency from 50 to 500 Hz for all wave forms.

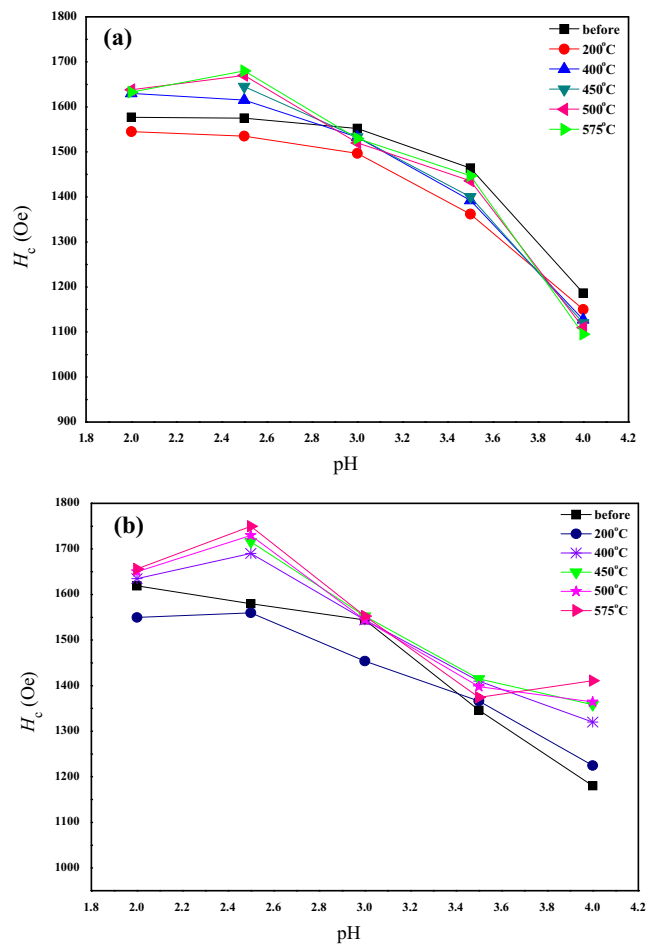


Fig. 10 Coercivity of a Co and b $\text{Co}_{0.95}\text{Al}_{0.05}$ nanowires as-deposited and annealed as a function of pH

Table 2 The out-of-plane coercivity of $\text{Co}_{1-x}\text{Al}_x$ nanowires for the as-deposited and annealed samples

Sample	pH	T (°C)					
		575	500	450	400	200	25
$\text{Co}_{0.99}\text{Al}_{0.01}$	1650	1665	1640	1624	1553	1597	2.0
	1670	1670	1645	1628	1503	1613	2.5
	1512	1508	1500	1477	1418	1485	3.0
	990	1027	1050	1049	1055	1100	3.5
	1079	1094	1130	1127	1150	1160	4.0
$\text{Co}_{0.97}\text{Al}_{0.03}$	1675	1684	1680	1680	1610	1634	2.0
	1700	1674	1670	1650	1530	1603	2.5
	1575	1571	1553	1550	1500	1539	3.0
	1195	1250	1265	1272	1210	1160	4.0

Subsequently, the effect of pH value on the magnetic properties of Co–Al nanowire arrays was investigated. It is well known that the texture configuration and the magnetic properties were varied by changing the pH value of the electrolyte [37]. The magnetic property of individual nanowire comes from the competing between the shape anisotropy and magnetocrystalline anisotropy. The shape anisotropy is assured when the demagnetizing factor controlled by aspect ratio is fixed, and the easy magnetization direction of the shape anisotropy is along the long axis of nanowire. Therefore, the easy magnetization direction of magnetocrystalline anisotropy of Co–Al nanowire arrays is an important factor to influence the magnetic properties.

To identify the influence of pH, the magnetic properties of Co and $\text{Co}_{1-x}\text{Al}_x$ sample alloy nanowires were measured before and after annealing. In Fig. 10, the coercivity was plotted versus pH for (a) Co and (b) $\text{Co}_{0.95}\text{Al}_{0.05}$, typically. The H_c data for all $\text{Co}_{1-x}\text{Al}_x$ alloys are tabulated in Table 2. As demonstrated in Fig. 10, the coercivity decreased with increasing pH for all annealing temperatures. It is accordance with Li et al.'s result that the structure of cobalt nanowire changes from fcc to hexagonal close-packed (hcp) structure by increasing the pH [38]. Moreover, for the hcp and fcc Co nanowires, magnetic measurements can provide a conclusive evidence on the easy axis as a result of different magnetocrystalline and shape anisotropies. For hcp-phase

Fig. 11 *a, b* A typical XRD patterns of the $\text{Co}_{0.95}\text{Al}_{0.05}$ nanowires fabricated at pH = 2.5 and 3.5 and annealed at 550 °C

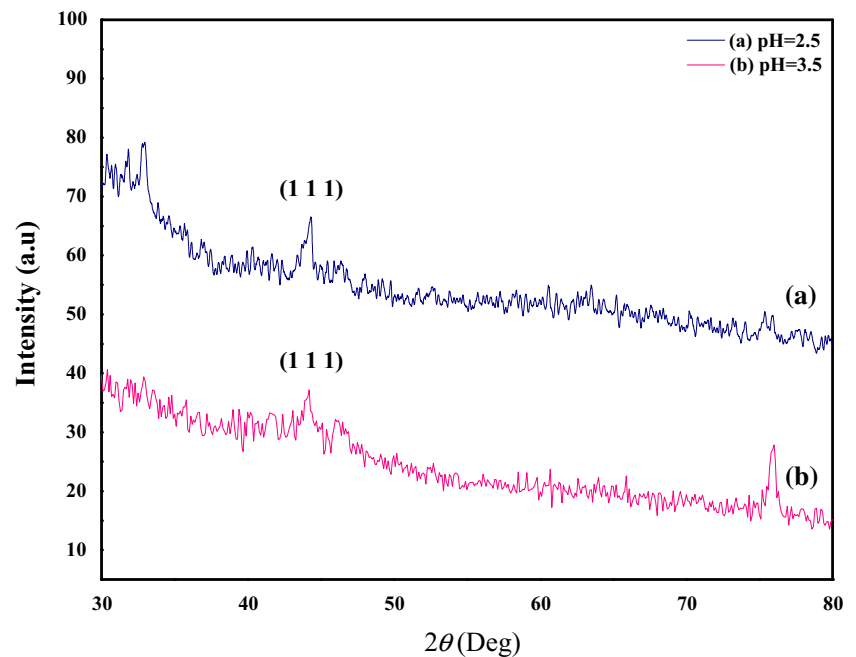


Table 3 The composition of the electrolyte used for electrodeposition of $(\text{Co}_{0.97}\text{Al}_{0.03})_{1-x}\text{Fe}_x$ nanowires

Sample	Concentration of $\text{CoSO}_4 \cdot 7\text{H}_2\text{O}$ (g/l)	Concentration of $\text{Al}_2(\text{SO}_4)_3 \cdot 18\text{H}_2\text{O}$ (g/l)	Concentration of $\text{FeSO}_4 \cdot 7\text{H}_2\text{O}$ (g/l)
$\text{Co}_{0.97}\text{Al}_{0.03}$	272.7	10.0	0.0
$(\text{Co}_{0.97}\text{Al}_{0.03})_{0.9}\text{Fe}_{0.1}$	245.4	9.0	27.8
$(\text{Co}_{0.97}\text{Al}_{0.03})_{0.7}\text{Fe}_{0.3}$	190.9	7.0	83.4
$(\text{Co}_{0.97}\text{Al}_{0.03})_{0.5}\text{Fe}_{0.5}$	136.3	5.0	139.0
$(\text{Co}_{0.97}\text{Al}_{0.03})_{0.3}\text{Fe}_{0.7}$	81.8	3.0	194.7
$(\text{Co}_{0.97}\text{Al}_{0.03})_{0.1}\text{Fe}_{0.9}$	27.3	1.0	250.2

Co, magnetocrystalline anisotropy energy density is comparable to the shape anisotropy energy density (5×10^6 against 6×10^6 erg/cm³, respectively) [39]. Therefore, the effective magnetic anisotropy should be determined by considering both magnetocrystalline anisotropy and shape anisotropy contributions. Actually, the exchange of the easy and hard axes by pH variations is further confirmed by magnetization measurements of the nanowires by Cho et al. [39], who showed that the easy axis is perpendicular to the nanowire. Therefore, the nanowire fabricated at pH = 4 in the present work is hcp, rather than fcc, because the fcc phase allows only the easy axis along the nanowire axis. Figure 11 shows the XRD pattern of $\text{Co}_{0.95}\text{Al}_{0.05}$ nanowires fabricated at pH = 2.5 and 3.5. Structurally, the peak around 44° could be fcc Co (1 1 1).

The Co–Al–Fe nanowire arrays were fabricated in AAO templates using the AC electrodeposition method similar for Co–Al with compositions such as $(\text{Co}_{0.97}\text{Al}_{0.03})_{1-x}\text{Fe}_x$ for

$x = 0$ to 90 (the concentration of the ions in the electrolytes is listed in Table 3).

Figure 12 shows the composition dependence of the coercivity and squareness of the magnetic hysteresis loops in parallel to the nanowire axis for $(\text{Co}_{0.97}\text{Al}_{0.03})_{1-x}\text{Fe}_x$ nanowires. As seen in this figure, H_c (||) has a small dependence on Fe content. The H_c (||) is proportional to the composition of Fe at low iron concentration. However, as the iron concentration rises higher than $x = 0.1$, the H_c drops slowly. It indicates that when the Fe composition is too high, the structure is similar to that of $\text{Co}_{0.97}\text{Al}_{0.03}$ phase. The value of H_c (||) increases from 1453 Oe (0 % Fe) to 1651 Oe (10 % Fe) with increasing Fe concentration and then decreases with more increasing in Fe content until a constant value is reached, i.e. 1520 Oe. Also, the squareness (M_r/M_s)(||) shows the same behavior as H_c , which increases from 0.80 (0 % Fe) to 0.95 (10 % Fe) and then decreases to 0.82.

Fig. 12 Coercivity and squareness (out-of-plane) of the $(\text{Co}_{0.97}\text{Al}_{0.03})_{1-x}\text{Fe}_x$ nanowire samples with different Fe concentrations deposited at 200 Hz and 30 Vpp in sine wave form

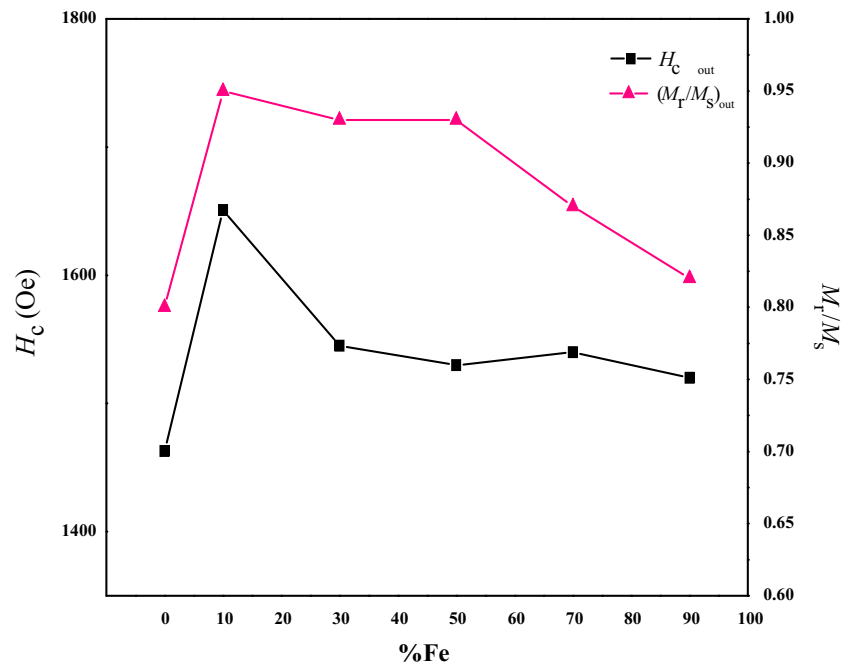


Fig. 13 Coercivity of $(\text{Co}_{0.97}\text{Al}_{0.03})_{1-x}\text{Fe}_x$ nanowires as a function of Fe concentration for different annealing temperatures

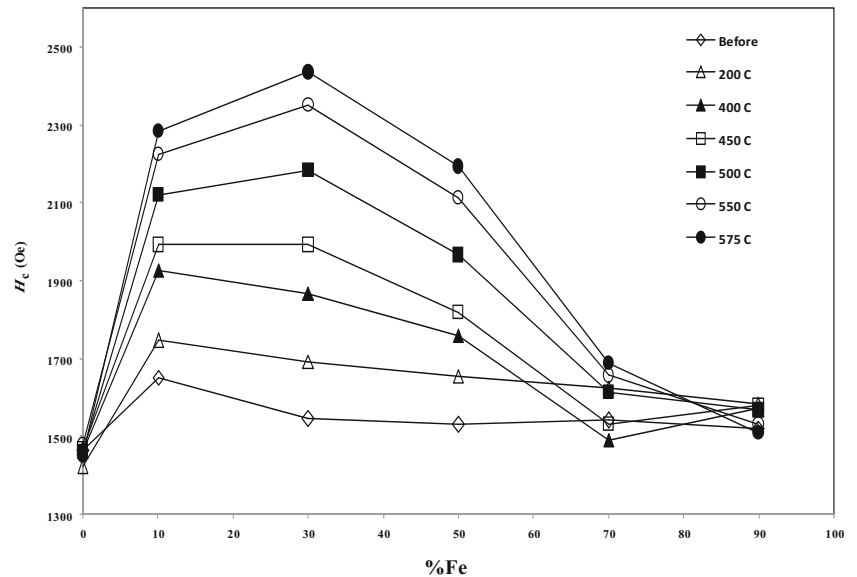


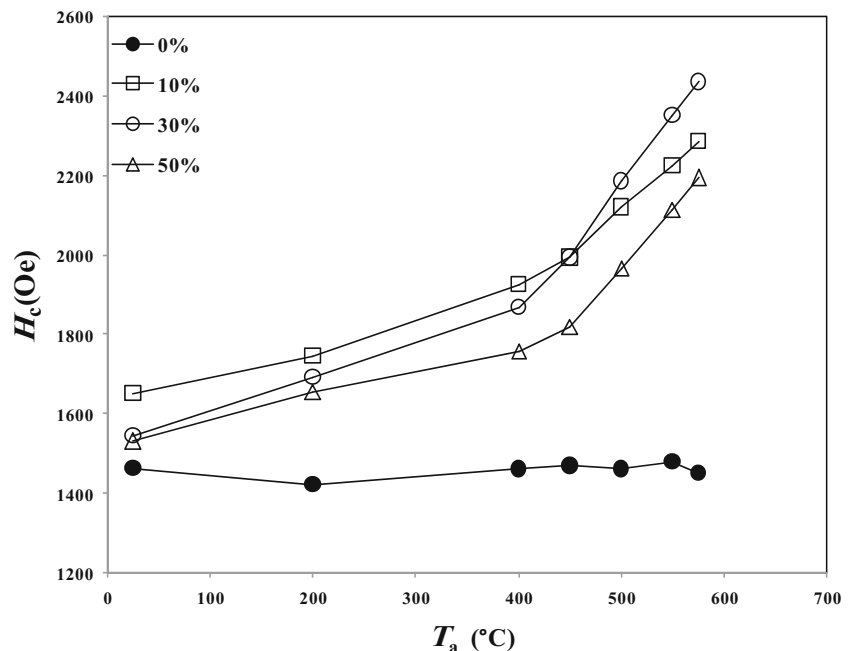
Figure 13 shows the relationships among H_c and the annealing temperature (T_a) of the $\text{Co}_{0.97}\text{Al}_{0.03}$ and $(\text{Co}_{0.97}\text{Al}_{0.03})_{1-x}\text{Fe}_x$ samples. It was found that the H_c of $\text{Co}_{0.97}\text{Al}_{0.03}$ was not changed with annealing significantly, while it strongly increases with increasing Fe content for $(\text{Co}_{0.97}\text{Al}_{0.03})_{1-x}\text{Fe}_x$ nanowire alloys. The value of the H_c reaches to a maximum at all annealing temperatures and then decreases with much increasing of Fe concentration.

On the other hand, the effects of annealing temperature on the H_c of $(\text{Co}_{0.97}\text{Al}_{0.03})_{1-x}\text{Fe}_x$ nanowires embedded in AAO measured at RT are shown in Fig. 14. The

result shows that coercivity increases with the enhancing of annealing temperature. One can notice that H_c of $(\text{Co}_{0.97}\text{Al}_{0.03})_{1-x}\text{Fe}_x$ nanowire arrays gently rises as T_a moves upward from 25 to 575 °C, but it remains constant for $\text{Co}_{0.97}\text{Al}_{0.03}$. This result indicates that annealing can change the H_c of $(\text{Co}_{0.97}\text{Al}_{0.03})_{1-x}\text{Fe}_x$ due to the improvement of the crystal quality and an increase of the grain size.

The increasing shape anisotropy, stress anisotropy and magnetocrystalline anisotropy after annealing of nanowires result in an increase of coercivity [40].

Fig. 14 Plot of the coercivity of $(\text{Co}_{0.97}\text{Al}_{0.03})_{1-x}\text{Fe}_x$ nanowires versus annealing temperature for different x values



4 Conclusions

In summary, the template method and electrodeposition techniques were employed for fabrication of arrays of nanowires of magnetic Co, Co–Al, and Co–Al–Fe alloys into the homemade AAO membranes. The effect of some parameters such as pH, annealing temperature, wave form, frequency, and composition of metals on magnetic properties of nanowire arrays was systematically studied. It was found that the crystalline structure nanowire arrays depend on the pH of electrolyte. The magnetization studies show that the coercivity of nanowires in the parallel geometry is larger than that of the perpendicular geometry. On the other hand, the magnetic property of nanowires change with respect to the aspect ratios, and their coercivity can be greatly enhanced by annealing. The as-prepared Co, Co–Al and Co–Al–Fe nanowires were observed by XRD to have a fcc structure with preferred orientation of (1 1 1) along the nanowire. The structure of the nanowires was found to have a strong influence on the magnetic properties, and the structure of nanowires changes from fcc to hcp structure by increasing the pH. The experimental results can be qualitatively explained after taking into account the shape and magnetocrystalline anisotropies.

Acknowledgments The authors are grateful to the Grant Research Council of the Hamedan University of Technology (HUT)

References

- Chang, S., Yoon, S., Park, H., Sakai, A.: *Mater. Lett.* **53**, 432–436 (2002)
- Walter, E.C., Ng, K., Zach, M.P., Penner, R.M., Favier, F.: *Microelectron. Eng.* **61–62**, 555–561 (2002)
- Nielsch, K., Wehrspohn, R.B., Barthel, J., Kirschner, J., Osele, U.G., Fischer, S.F., Kronmuller, H.: *Appl. Phys. Lett.* **79**, 1360–1362 (2001)
- Ross, C., Chantrell, R., Hwang, M., Farhoud, M., Savas, T., Hao, Y., Smith, H., Ross, F., Redjal, M., Himpfrey, F.: *Phys. Rev. B* **62**, 14252 (2000)
- Cho, S.G., Yoo, B., Kim, K.H., Kim, J.: *IEEE T. Magn.* **46**, 420–423 (2010)
- He, Z., Zheng, M., Hao, M., Zhou, T., Ma, L., Shen, W.: *Appl. Phys. A* **104**, 89–94 (2011)
- Nasirpour, F.: *IEEE T. Magn.* **47**, 2015–2021 (2011)
- Iselt, D., Gaitzsch, U., Oswald, S., Fähler, S., Schultz, L., Schlörb, H.: *Electrochim. Acta* **56**, 5178–5183 (2011)
- Cortés, M., Serrà, A., Gómez, E., Vallés, E.: *Electrochim. Acta* **56**, 8232–8238 (2011)
- Routkevitch, D., Tager, A.A., Haruyama, J., Almawlawi, D., Moskovits, M., Xu, J.M.: *IEEE Trans. Electron. Devices* **43**, 1646–1658 (1996)
- Cui, B.Z., Gonzales, B., Marinescu, M., Liu, J.F.: *IEEE T. Magn.* **49**, 3326–3329 (2013)
- Najafi, M., Assari, P., Rafati, A.A., Hamehvaisy, M.: *J. Superconduct. Novel Magnet.* **27**, 2821–2827 (2014)
- Najafi, M., Alemipour, Z., Hasanzadeh, I., Aftabi, A., Soltanian, S.: *J. Superconduct. Novel Magnet.* **28**, 95–101 (2015)
- Jaleh, B., Omidvar Dezfuli, A., Jaberian Hamedan, V., Najafi, M., Tamari, E.: *Inter. J. Phys. Sci.* **6**, 4775–4780 (2011)
- Najafi, M., Soltanian, S., Danyali, H., Hallaj, R., Salimi, A., Elahi, S.M., Servati, P.: *J. Mater. Res.* **27**, 2382–2390 (2012)
- Hajian, A., Rafati, A.A., Afraz, A., Najafi, M.: *J. Electrochem. Soc.* **161**, B196–B200 (2014)
- Hamidi, S.M., Sobhani, A., Aftabi, A., Najafi, M.: *J. Magnet. Magnet. Mater.* **374**, 139–143 (2015)
- Najafi, M., Rafati, A.A., Khorshidi Fart, M., Zare, A.: *J. Mater. Res.* **29**, 190–196 (2014)
- Cao, L., Qiu, X., Ding, J., Li, H., Chen, L.: *J. Mater. Sci.* **41**, 2211–2218 (2006)
- Wang, Y.W., Meng, G.W., Liang, C.H., Wang, G.Z., Zhang, L.D.: *Chem. Phys. Lett.* **339**, 174–178 (2001)
- Wang, Y.W., Wang, G.Z., Wang, S.X., Gao, T., Sang, H., Zhang, L.D.: *Appl. Phys. A* **74**, 577–580 (2002)
- Chiriac, H., Dragos, O.G., Grigoras, M., Ababei, G., Lupu, N.: *IEEE T. Magn.* **45**, 4077–4080 (2009)
- Xie, Y., Zhang, J.M.: *J. Phys. Chem. Solids* **73**, 530–534 (2012)
- Chen, C.C., Toyoshima, H., Hashimoto, M., Shi, J., Nakamura, Y.: *Appl. Phys. A* **81**, 127–130 (2005)
- Ji, G., Tang, S., Chen, W., Gu, B., Du, Y.: *Solid State Commun.* **132**, 289–292 (2004)
- Su, Y.K., Qin, D.H., Zhang, H.L., Li, H., Li, H.L.: *Chem. Phys. Lett.* **388**, 406–410 (2004)
- Schwarzacher, W., Kasyutich, O.I., Evans, P.R., Darbyshire, M.G., Yi, G., Fedosyuk, V.M., Rousseaux, F., Cambil, E., Decanini, D.: *J. Magn. Magn. Mater.* **198–199**, 185–190 (1999)
- Dalchiele, E.A., Marotti, R.E., Cortes, A., Riveros, G., Gómez, H., Martínez, L., Romero, R., Leinen, D., Martin, F., Ramos-Barrado, J.R.: *Physica E* **37**, 184–188 (2007)
- Tang, S.L., Chen, W., Lu, M., Yang, S.G., Zhang, F.M., Du, Y.W.: *Chem. Phys. Lett.* **384**, 1–4 (2004)
- Tang, X.T., Wang, G.C., Shima, M.: *J. Magn. Magn. Mater.* **309**, 188–196 (2007)
- Liu, L.F., Zhou, W.Y., Xie, S.S., Albrecht, O., Nielsch, K.: *Chem. Phys. Lett.* **466**, 165–169 (2008)
- Fang, T.H., Wang, T.H., Liu, C.H., Ji, L.W., Kang, S.H.: *Nanoscale Res. Lett.* **2**, 410–415 (2007)
- Gao, D., Shi, Z., Xu, Y., Zhang, J., Yang, G., Zhang, J., Wang, X., Xue, D.: *Nanoscale Res. Lett.* **5**, 1289–1294 (2010)
- Bantu, A.K.M., Rivas, J., Zaragoza, G., Quintela, M.A.L., Blanco, M.C.: *J. Appl. Phys.* **89**, 3393–3397 (2001)
- Gao, J.H., Zhan, Q.F., He, W., Sun, D.L., Cheng, Z.H.: *J. Magn. Magn. Mater.* **305**, 365–371 (2006)
- Rosa, W.O., Vivas, L.G., Pirota, K.R., Asenjo, A., Vazquez, M.: *J. Magn. Magn. Mater.* **324**, 3679–3682 (2012)
- Ren, Y., Liu, Q.F., Li, S.L., Wang, J.B., Han, X.H.: *J. Magn. Magn. Mater.* **321**, 226–230 (2009)
- Li, F., Wang, T., Ren, L., Sun, J.: *J. Phys. Condens Mater.* **16**, 8053–8060 (2004)
- Cho, J.U., Wu, J.H., Min, J.H., Ko, S.P., Soh, J.Y., Liu, Q.X., Kim, Y.K.: *J. Magn. Magn. Mater.* **303**, e281–e285 (2006)
- Fu, J.L., Yan, Z.J., Xu, Y., Fan, X.L., Xue, D.S.: *J. Phys. Chem. Solids* **68**, 2221–2226 (2012)